The *Neurospora crassa* exocyst complex tethers Spitzenkörper vesicles to the apical plasma membrane during polarized growth

Meritxell Riquelme[a], Erin L. Bredeweg[b,*], Olga Callejas-Negrete[a,*], Robert W. Roberson[c], Sarah Ludwig[d], Alejandro Beltrán-Aguilar[a], Stephan Seiler[d], Peter Novick[e], and Michael Freitag[b]

[a]Department of Microbiology, Center for Scientific Research and Higher Education of Ensenada, Ensenada, BC 22860, Mexico; [b]Department of Biochemistry and Biophysics, Center for Genome Research and Biocomputing, Oregon State University, Corvallis, OR 97331; [c]School of Life Sciences, Arizona State University, Tempe, AZ 85287; [d]Department of Molecular Plant Physiology, Institute for Biologie II, Albert-Ludwigs University Freiburg, 79104 Freiburg, Germany; [e]Department of Cellular and Molecular Medicine, University of California, San Diego, La Jolla, CA 92093

ABSTRACT Fungal hyphae are among the most highly polarized cells. Hyphal polarized growth is supported by tip-directed transport of secretory vesicles, which accumulate temporarily in a stratified manner in an apical vesicle cluster, the Spitzenkörper. The exocyst complex is required for tethering of secretory vesicles to the apical plasma membrane. We determined that the presence of an octameric exocyst complex is required for the formation of a functional Spitzenkörper and maintenance of regular hyphal growth in *Neurospora crassa*. Two distinct localization patterns of exocyst subunits at the hyphal tip suggest the dynamic formation of two assemblies. The EXO-70/EXO-84 subunits are found at the peripheral part of the Spitzenkörper, which partially coincides with the outer macrovesicular layer, whereas exocyst components SEC-5, -6, -8, and -15 form a delimited crescent at the apical plasma membrane. Localization of SEC-6 and EXO-70 to the plasma membrane and the Spitzenkörper, respectively, depends on actin and microtubule cytoskeletons. The apical region of exocyst-mediated vesicle fusion, elucidated by the plasma membrane–associated exocyst subunits, indicates the presence of an exocytotic gradient with a tip-high maximum that dissipates gradually toward the subapex, confirming the earlier predictions of the vesicle supply center model for hyphal morphogenesis.

INTRODUCTION

Exocytosis constitutes the last stage of the secretory pathway. It is a key process for cell growth and morphogenesis and entails the fusion of secretory vesicles to the plasma membrane (PM) to maintain the normal complement of proteins and lipids at specific PM subdomains (Shandala *et al.*, 2012). During exocytosis, the vesicle membrane fuses with the PM via a fusion pore that dilates until the secretory vesicle collapses into the PM and the contents of the vesicles are deposited into the extracellular space (Rizzoli and Jahn, 2007).

The exocyst, a conserved multiprotein complex required for the final steps of exocytosis (Novick *et al.*, 1980, 1981; Hsu *et al.*, 2004), tethers vesicles to the PM before their soluble *N*-ethylmaleimide–sensitive factor attachment protein receptor (SNARE)–dependent fusion at specific PM sites (TerBush and Novick, 1995) and consists of eight components: Sec3p, Sec5p, Sec6p, Sec8p, Sec10p, Sec15p, Exo70p, and Exo84p (TerBush *et al.*, 1996; Guo *et al.*, 1999a,b). All exocyst subunits are encoded by single genes in fungi and animals, whereas plants often have several genes for individual components (Elias *et al.*, 2003; Zhang *et al.*, 2010). It was suggested

that this expansion of exocyst-encoding genes in plants might reflect differential expression during development in various tissues or multiple types of exocytosis (Zhang *et al.*, 2010).

All exocyst components are hydrophilic, cytosolic proteins, which can also associate with membranes (TerBush and Novick, 1995). In *Saccharomyces cerevisiae*, exocyst components are localized at the site of bud emergence and the tip of small daughter cells and relocate to the mother–daughter connection during progression of the cell cycle (TerBush and Novick, 1995; TerBush *et al.*, 1996; Finger *et al.*, 1998). The exocyst complex regulates the docking of vesicles to specific sites of the PM during polarized secretion. The exocyst complexes of plants and mammals have more-diversified roles than that of budding yeast (Wang and Hsu, 2006; Zhang *et al.*, 2010). In undifferentiated neuronal cells, for example, the exocyst shows perinuclear localization, but on differentiation it is redistributed to the extending neurite and concentrates at the growth cone (Vega and Hsu, 2001). In epithelial cells, the exocyst accumulates at the level of the adherens junction (Grindstaff *et al.*, 1998). As in yeast, the mammalian exocyst is also essential for cellular processes that require polarized membrane traffic (Hertzog and Chavrier, 2011). The exocyst complex exists as two subcomplexes in yeast and mammalian cells, and the interaction between the two assemblies allows vesicle docking to the PM (Wang and Hsu, 2006). In yeast, Exo70p and Sec3p components are tethered to the PM (Boyd *et al.*, 2004), whereas the remaining exocyst subunits associate with secretory vesicles through Sec4p (Guo *et al.*, 1999b), a Rab GTPase that controls assembly of the exocyst, and the vesicle-SNARE Snc1p/Snc2p (Shen *et al.*, 2013). In mammals the PM-associated subcomplex contains Exo70, Sec3, Sec5, Sec6, and Sec8, whereas Sec10, Sec15 and Exo84 are complexed at the vesicle membrane (Moskalenko *et al.*, 2003). Coassembly of the two animal subcomplexes is governed by the Ral-GTPases RalA and RalB via their interaction with Sec5 and Exo84 (Moskalenko *et al.*, 2003). In plants there is less information on where exocyst subunits localize (Zhang *et al.*, 2010). Immunolocalization studies in tobacco pollen tubes showed SEC6, SEC8, EXO70, and EXO70A1 at tip regions (Hala *et al.*, 2008). In *Arabidopsis*, the exocyst facilitates initiation and maintenance of polarized growth in pollen tubes (Cole *et al.*, 2005) and participates in secretory processes during cytokinesis (Fendrych *et al.*, 2010).

Although the basic exocytotic machinery is conserved among eukaryotes, organisms have evolved different strategies to regulate endomembrane traffic. In contrast to unicellular yeasts, in which growth is directed to the bud tip and site of cell division in a cell cycle–dependent manner, in tip-growing cells, such as root hairs, pollen tubes, and developing neurons, expansion occurs primarily at the tip. Thus polarized exocytosis at sites of cell growth must be maintained permanently. Sustained exocytosis is focused to the hyphal apex of filamentous fungi, where a Spitzenkörper collects secretory vesicles temporarily, from which they are delivered to the apical PM (Bartnicki-García *et al.*, 1989). The localization of exocyst components was correlated with the hyphal growth rate in a filamentous member of the Saccharomycotina, *Ashbya gossypii* (Köhli *et al.*, 2008). *Ag*Sec3, *Ag*Sec5, and *Ag*Exo70 localized as a cortical cap at the hyphal tip of slow-growing hyphae, whereas in fast-growing hyphae they accumulated at the Spitzenkörper. In the dimorphic yeast *Candida albicans*, exocyst components Sec3, 6, 8, 15, Exo70, and Exo84 localized to an apical crescent and remained stably located (Jones and Sudbery, 2010; Sudbery, 2011). In *Aspergillus nidulans*, SECC, the homologue of Sec3p, was localized in a small region of the PM, immediately anterior to the Spitzenkörper, at the apices of fast-growing hyphae (Taheri-Talesh *et al.*, 2008). In *Aspergillus oryzae*, AoSec3 was localized to cortical caps at the hyphal tip

as in *A. nidulans* but was also found in septa (Hayakawa *et al.*, 2011).

Neurospora crassa, one of the fastest tip-growing organisms, has single genes for all eight exocyst components (Borkovich *et al.*, 2004; Riquelme *et al.*, 2011). Hyphae of *N. crassa* present a multilayered Spitzenkörper with a core of microvesicles that contain chitin synthase and an outer layer of macrovesicles that contain glucan synthase activity (Verdin *et al.*, 2009; Sánchez-León *et al.*, 2011). To study the final steps of the secretory pathway for these vesicles and their cargoes, we constructed translational fusions of the exocyst-encoding genes with *gfp* at their endogenous loci and analyzed their expression in relation to Spitzenkörper components.

RESULTS

Identification of *N. crassa* exocyst complex

Genes encoding putative *N. crassa* exocyst components were identified by in silico analysis of the *N. crassa* genome (www.broadinstitute.org/annotation/genome/neurospora/MultiHome.html; Galagan *et al.*, 2003) with fungal plant and human exocyst proteins as "bait" (Table 1). Eight clear homologues of exocyst proteins were identified and named SEC-3, -5, -6, -8, -10, and -15 and EXO-70 and -84. In addition, we found one gene (NCU03658) with a truncated Sec10-like motif, encoding the homologue of secretory pathway protein Sls2/Rcy1 (Figure 1). Overall, amino acid conservation of exocyst subunits between *S. cerevisiae* and *N. crassa* subunits is low (14–24% identity; Table 1). As one would expect, conservation is higher when comparing *Ashbya gossypii* to *S. cerevisiae* and *N. crassa* to *A. nidulans* proteins, respectively.

All exocyst components but *sec-10* were tagged with the split marker technique (Supplemental Figure S1 and *Materials and Methods*). The modified green fluorescent protein (GFP) fusion proteins expressed from the endogenous loci were functional, and all generated strains displayed wild-type (WT) morphology. To determine the composition of the *N. crassa* exocyst, we performed GFP-trap affinity purification experiments coupled to mass spectrometry (AP-MS). These AP-MS raw data (Supplemental Table S1) were filtered against a control data set obtained from purifications with GFP-expressing cells and precipitates of GFP-tagged proteins that have functions unrelated to the exocyst (Dettmann *et al.*, 2013; Heilig *et al.*, 2013). Precipitates of the six tagged exocyst subunits SEC-3, -5, -6, and -8 and EXO-70 and -84 recovered the entire octameric complex (Table 2). SEC-15 could not be precipitated. No additional proteins were identified that copurified with all exocyst components in a stable manner, and most proteins identified in these preparations were obvious contaminants. On the basis of these data, we conclude that an octameric exocyst complex exists in *N. crassa*.

Exocyst subunits display two distinct localization patterns at the hyphal apex

The tagged exocyst components were detected primarily at two cellular locations at the hyphal apex: the Spitzenkörper outer layer and apical PM (Figure 2). In addition, we observed some cytoplasmic fluorescence, probably representing a fraction of cytosolic components. Exocyst components SEC-5, -6, -8 ,and -15 accumulated primarily as a PM crescent at the hyphal dome and were excluded from the FM4-64–stained Spitzenkörper (Figure 2 and Supplemental Figure S2). In contrast, EXO-70 and EXO-84 accumulated in the proximal region of the external layer of the Spitzenkörper (Figure 2 and Supplemental Figure S2). SEC-3 accumulated at both the crescent and the Spitzenkörper outer layer, suggesting that it

Component	Locus ID	Subcellular localization	Identity with Sc (%)[a]	Identity with Nc (%)	Reference
		N. crassa			
sec-3	NCU09869	Between Spk outer layer and PM	14	N/A	This study
sec-5	NCU07698	Surface crescent	20	N/A	This study
sec-6	NCU03341	Surface crescent	21	N/A	This study
sec-8	NCU04190	Surface crescent	19	N/A	This study
sec-10	NCU09313	–	24	N/A	–
sec-15	NCU00117	Surface crescent	22	N/A	This study
exo-70	NCU08012	Spk outer layer	23	N/A	This study
exo-84	NCU06631	Spk outer layer	20	N/A	This study
		A. nidulans			
secC (sec3)	AN0462.2	Surface crescent	17	36	Taheri-Talesh *et al.* (2008)
secE (sec5)	AN1002.2		20	48	–
secF (sec6)	AN1988.2		22	50	–
secH (sec8)	AN11007.2		20	41	–
secJ (sec10)	AN8879.2		25	50	–
secO (sec15)	AN6493.2		24	63	–
exo70	AN6210.2		23	45	–
exo84	AN0560.2		22	46	–
		S. cerevisiae			
SEC3	YER008C	Bud, cell periphery, bud neck	N/A	14	Finger *et al.* (1998)
SEC5	YDR166C	Bud, cell periphery, bud neck	N/A	20	Boyd *et al.* (2004)
SEC6	YIL068C	Bud, cell periphery, bud neck	N/A	21	TerBush and Novick (1995)
SEC8	YPR055W	Bud, cytoplasm, bud neck	N/A	20	TerBush and Novick (1995)
SEC10	YLR166C	Bud, cell periphery, bud neck	N/A	24	Boyd *et al.* (2004)
SEC15	YGL233W	Bud, cytoplasm, cell periphery	N/A	22	TerBush and Novick (1995)
EXO70	YJL085W	Bud, bud neck	N/A	24	Boyd *et al.* (2004)
EXO84	YBR102C	Bud, cell periphery, bud neck	N/A	18	Guo *et al.* (1999a)
		A. gossypii			
Agsec3	ADR012C	S, Surface crescent F, Spk	31	15	Köhli *et al.* (2008)
Agsec5	AGL158C	S, Surface crescent F, Spk	49	25	Köhli *et al.* (2008)
Agsec6	ACL047W		54	24	–
Agsec8	ADL317C		40	24	–
Agsec10	AGL130C		47	25	–
Agsec15	AFR251C		52	23	–
Agexo70	AFR100W	S, Surface crescent F, Spk	51	22	Köhli *et al.* (2008)
Agexo84	ADL321W		46	21	–

Percentage identity of exocyst subunit protein sequence compared with *S. cerevisiae* (Sc) and *N. crassa* (Nc). Based on identity and coverage of the aligned regions (usually 80–100%), Sec3 is the least-conserved exocyst component (coverage in various comparisons, 46–83%). Spk, Spitzenkörper; S, slow; F, fast.
[a]bl2seq (http://blast.ncbi.nlm.nih.gov/Blast.cgi) was used to align sequence pairs. Exact amino acid identities of all aligned hits were summed and divided by the total length of the protein in the corresponding organism to get the final percentage.

TABLE 1: Exocyst components and their localization from four members of the Ascomycota that serve as model organisms: two Pezizomycotina (*N. crassa* and *A. nidulans*) and two Saccharomycotina (*S. cerevisiae* and *A. gossypii*).

may be the component bringing the remaining subunits together (Figure 2).

Coexpression of SEC-6 and EXO-70 labeled with either GFP or mCherry showed lack of colocalization of these two subunits (Supplemental Figure S3). Therefore SEC-6 and EXO-70 were chosen as representative markers for the two putative exocyst localizations—plasma membrane and Spitzenkörper outer layer (Supplemental Figure S3)—for further experiments. Both proteins showed positional changes within the *N. crassa* apex that correlated with changes in the position of the Spitzenkörper and thus determined growth

FIGURE 1: Exocyst components of *N. crassa*. Exocyst domains, designated SEC or EXO, were identified in the Protein Data Bank database by BLAST or by domain identification at the *Neurospora crassa* Database (www.broadinstitute.org/annotation/genome/neurospora/MultiHome.html). Coiled-coil domains and globular domains (GlobPlot) were identified with Eukaryotic Linear Motif (http://elm.eu.org/). Coiled-coil prediction was done by COILS in window sizes of 7, 14, 21, and 28 amino acids (http://npsa-pbil.ibcp.fr/cgi-bin/npsa_automat.pl?page=npsa_lupas.html). The globular domains represent ordered portions of the protein; multiple coiled-coil motifs suggest a repeating pattern, which may result in stacking of exocyst components in vertical columns, as suggested by previous electron microscope studies and protein structure predictions (Munson and Novick, 2006). Proteins are represented top to bottom as SEC-3, -5, -6, -8, -10, -10*, and -15 and EXO-70 and -84 (Table 2). SEC-10* contains a C-terminally truncated domain with homology to SEC-10.
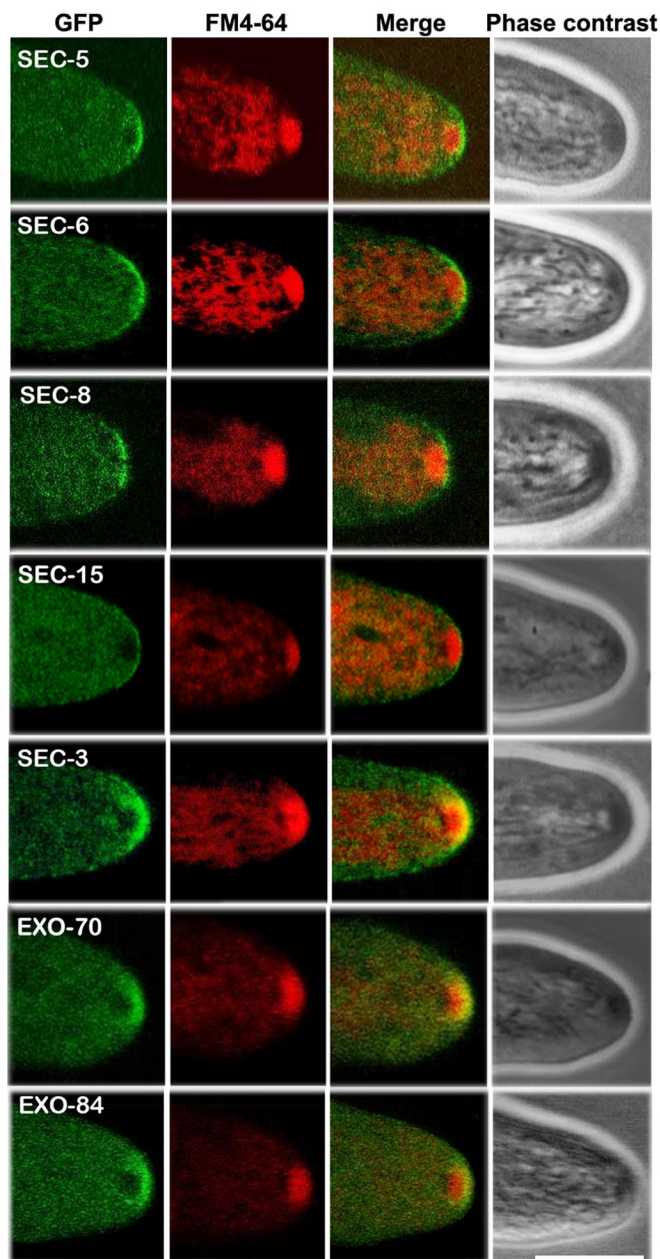

FIGURE 2: Localization of exocyst components at apices of mature hyphae of *N. crassa* imaged by laser scanning confocal microscopy. For details see text. First column, GFP fluorescence; second column, FM4-64–stained cells; third column, merged; fourth column, phase contrast. Note that exocyst components EXO-70 and EXO-84 partially colocalize with the frontal outer part of the FM4-64–stained Spitzenkörper. Scale bar, 10 μm.

directionality (Figure 3). No correlation between localization pattern of SEC-6-GFP and EXO-70-GFP and the tip extension rates was observed (Figure 3). In slow-growing hyphae of strains expressing SEC-6-GFP the fluorescence had a tendency to be more spread out, but it was always distributed to form an apical crescent (Figure 3). In germlings, there was a weaker and smaller fluorescent crescent at the apices of SEC-3-GFP, SEC-5-GFP, SEC-6-GFP, SEC-8-GFP, EXO-70-GFP, and EXO-84-GFP (Supplemental Figure S4). No fluorescence was observed at the apex of germ tubes for SEC-15-GFP (unpublished data).

Because components of the exocyst complex are concentrated in subdomains of the PM that represent sites of active vesicle fusion (TerBush and Novick, 1995; Hertzog and Chavrier, 2011), we analyzed the behavior of SEC-6-GFP by total internal reflection fluorescence microscopy (TIRFM). TIRFM allowed detection of

N. crassa exocyst component	Identified by GFP-trap + MS in:					
	SEC3-GFP	SEC5-GFP	SEC6-GFP	SEC8-GFP	EXO70-GFP	EXO84-GFP
SEC-3	**37/52**	30/40	42/53	32 /42	36/45	35/45
SEC-5	44/38	**40/34**	45/38	34/31	46/39	43/35
SEC-6	39/28	43/30	**33/22**	32/21	43/34	32/21
SEC-8	45/44	41/37	46/47	**37/34**	46/46	40/37
SEC-10	44/35	41/32	38/32	36 /27	43/35	41 /33
SEC-15	41/26	40/24	35/24	31/21	43/28	34/23
EXO-70	45/27	35/19	44/22	40/21	**50/24**	30/16
EXO-84	42/27	42/27	35/21	30/18	32/20	**48/32**

Percentage protein coverage/number of identified unique peptides in GFP-trap + MS analysis. Bold numbers indicate the GFP-fusion protein used as bait.

TABLE 2: Proteomics analysis of the *N. crassa* exocyst complex.
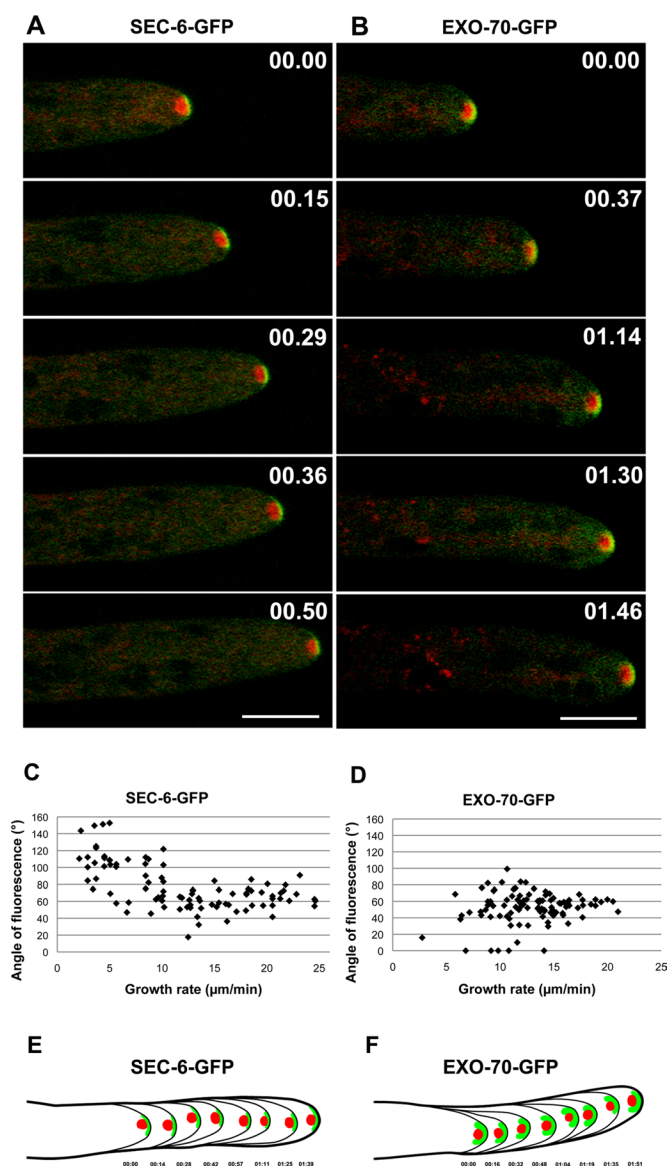

FIGURE 3: Positional changes of exocyst components SEC-6 and EXO-70 during hyphal growth of *N. crassa*. Fluorescence position of both SEC-6-GFP (A) and EXO-70-GFP (B) changes as the hyphal apex changes direction of growth. Scale bars, 10 µm. Time in minutes:seconds. Angle of fluorescence is plotted against growth rate (µm/min) of hyphae expressing SEC-6-GFP (C) or EXO-70-GFP (D). N = 90. Schematic representation of several hyphal profiles from a time series showing the position of GFP-tagged exocyst components SEC-6 (E) or EXO-70 (F) and corresponding changes in position of the Spitzenkörper stained with FM4-64. Time in minutes:seconds.

fluorescence-tagged proteins that are very close to the cell surface in regions of the hyphae in close contact with the coverslip. High-intensity fluorescent clusters, which represent individual exocytic events, were detected at delimited locations within the apical PM (Figure 4 and Supplemental Movie S1), suggesting an orderly discontinuous vesicle discharge mechanism for exocytosis during tip growth. These exocytic events were further evidenced when the times series obtained by TIRFM were converted into surface plots (Supplemental Movie S2).

The vesicle-associated exocyst components colocalize with the macrovesicular outer layer of the Spitzenkörper in an actin- and microtubule-dependent manner

We previously showed that the *N. crassa* Spitzenkörper consists of functionally and structurally distinct layers of vesicles (Verdin *et al.*, 2009). To analyze the role of the exocyst complex in tethering of the different populations of vesicles at the Spitzenkörper, we coexpressed the GFP-tagged exocyst components SEC-6 or EXO-70 in strains with CHS-1–mCherry fluorescent protein (mChFP; microvesicular Spitzenkörper core) and strains with GS-1-mChFP (macrovesicular Spitzenkörper outer layer). The vesicle-associated component EXO-70 did not colocalize with the Spitzenkörper core labeled with CHS-1-mChFP but partially colocalized with the Spitzenkörper outer layer, occupied by the glucan synthase regulator GS-1-mChFP (Figure 5 and Supplemental Figure S5). The PM-associated component SEC-6, in contrast, did not colocalize with any layer of the Spitzenkörper (Figures 2 and 5, Supplemental Figure S5, and Supplemental Movie S3).

The localization of EXO-70-GFP was impaired upon exposure to the secretory pathway inhibitor brefeldin A (BFA; Figure 6), consistent with the association of this exocyst component with secretory vesicles. In contrast, SEC-6-GFP remained at the hyphal apical plasma membrane after drug treatment (Figure 6), providing additional support for incorporation of this exocyst component at plasma membrane independently of the secretory pathway.
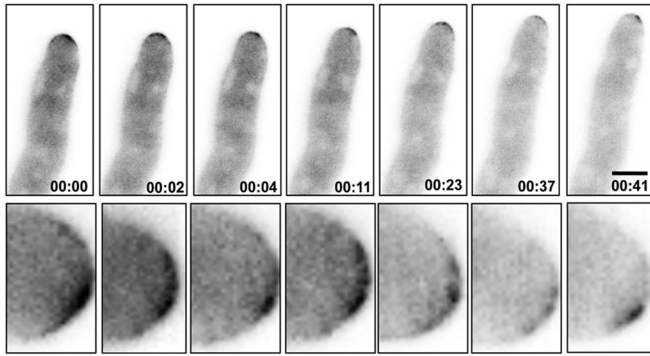
FIGURE 4: Individual frames extracted from a TIRFM time series of a *N. crassa* hypha expressing SEC-6-GFP. Bursts of exocytosis occurring at different positions within the apical plasma membrane can be observed. Bottom, magnified apices of the corresponding panels. Scale bar, 10 μm. Time in minutes:seconds.

To address the importance of the cytoskeleton for the localization of the two exocyst subunits, we determined the behavior of SEC-6-GFP and EXO-70-GFP after depolymerization of the actin and microtubule (MT) cytoskeletons. The effects of each inhibitor on growth and morphology of *N. crassa* hyphae were previously reported (Riquelme *et al.*, 2000, 2002). Both SEC-6 and EXO-70 required the actin and the MT cytoskeletons for proper localization (Figure 7). On benomyl treatment, the apical localization of SEC-6-GFP was retained when hyphae started curling and lost growth directionality, although only very weak and dispersed fluorescence could be observed. After treatment with latrunculin A, hyphae ceased to grow in a polar manner and started to swell. During that period no SEC-6-GFP could be seen at the apical PM (unpublished data). When the hyphae started recovering and growth resumed apically, SEC-6-GFP was again observed at the apical PM (Figure 7, arrowhead). EXO-70-GFP also required both the microtubule and the actin cytoskeleton for proper localization. Both benomyl and latrunculin A treatments hindered localization of EXO-70 at the Spitzenkörper.

An intact exocyst complex is necessary for organization of the Spitzenkörper and regular hyphal growth

The *N. crassa* functional genome project (Colot *et al.*, 2006) generated deletion mutants for *sec-5*, *sec-8*, *sec-10*, *sec-15*, *exo-70*, and *exo-84* (available from the Fungal Genetics Stock Center [FGSC], Kansas City, MO; see Table 3). Homokaryotic deletion mutants were available for *sec-5* but could not be obtained for any of the remaining exocyst components, suggesting that these genes are essential. Although viable, the growth of *N. crassa* Δ*sec-5* was highly disturbed. with a phenotype similar to that previously described for *sec-5*[7-9], a mutant strain obtained by ultraviolet mutagenesis (Seiler and Plamann, 2003). We sequenced the *sec-5* locus in this strain and found several nucleotide insertions that introduced a nonsense codon early in the sequence, suggesting that *sec-5*[7-9] represents a loss-of-function mutant. Both Δ*sec-5* and *sec-5*[7-9] grew as highly compact, button-like colonies, in contrast to the spreading colony appearance typical of the WT strain (Figure 8, A and C). At low magnification, Δ*sec-5* and *sec-5*[7-9] produced hyperbranched and distorted hyphae (Figure 8, D and F).

WT hyphae stained with FM4-64 showed fluorescence at the plasma membrane (PM) and in apical vesicles that were concentrated at the Spitzenkörper (Figure 8J). Δ*sec-5* and *sec-5*[7-9] mutants
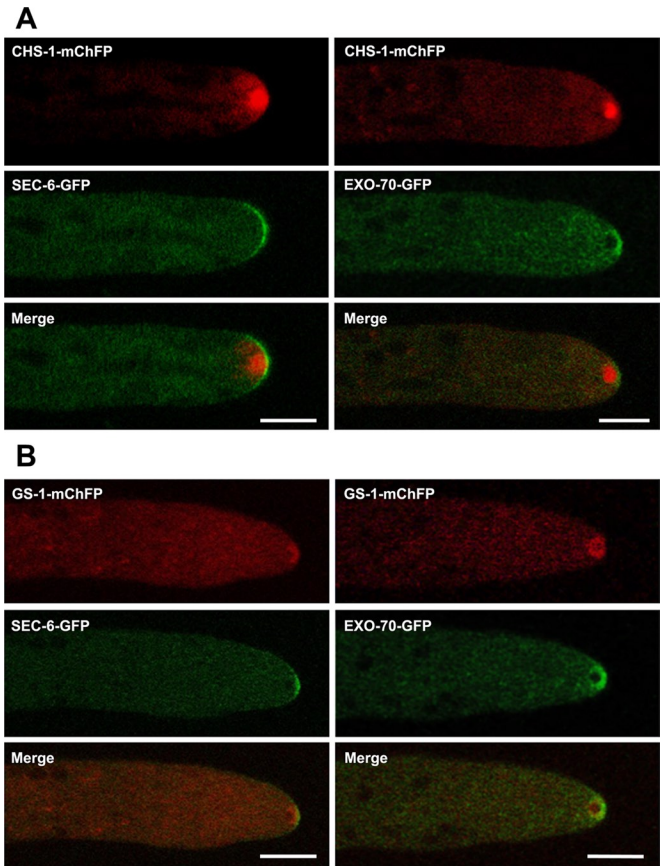

FIGURE 5: Coexpression of exocyst components and Spitzenkörper components. (A) Exocyst components SEC-6 and EXO-70 do not colocalize with chitin synthase CHS-1, although EXO-70-GFP can be found surrounding CHS-1-mChFP at the core of the Spitzenkörper. (B) SEC-6 and the glucan synthase regulator GS-1 do not colocalize, whereas EXO-70 and GS-1 are partially colocalized. Scale bars, 10 μm.

showed lower accumulation of FM4-64 fluorescence at the tip (Figure 8, K and L), indicative of a lower concentration of vesicles. In fact, *N. crassa* Δ*sec-5* and *sec-5*[7-9] did not form a Spitzenkörper under phase-contrast microscopy (Figure 8, H and I). This observation was further investigated by transmission electron microscopy. In wild-type *N. crassa* hyphae, the Spitzenkörper was composed of an aggregation of macrovesicles (vesicles ranging from 70 to 100 nm in diameter) surrounding a differentiated core region composed of microvesicles (vesicles ranging from 25 to 40 nm in diameter) embedded in a dense granular to fibrous matrix, most likely actin microfilaments (Figure 9, A and B). Macrovesicles in wild-type hyphae contained a fine, granular, electron-opaque matrix (Figure 9, B and D) and had on average a diameter of 83 nm ($n = 109$; SD = 8.5). Directly subtending the Spitzenkörper was a cluster of ribosomes (Figure 9B). Ribosomes were also present within the core but were less commonly observed there. Microvesicles were on average 32 nm in diameter ($n = 217$; SD = 4.2) and were spherical when viewed in thin section (Figure 9, B and D). Occasionally, microvesicles were polyhedral. Macrovesicles and microvesicles extended into the apical cortex (Figure 9, A, C, and D), and, on occasion, macrovesicles were noted in juxtaposition to the cytosolic surface of the apical PM (i.e., docked; Figure 9C). Invaginations of the apical PM seen at the hyphal apex (Figure 9D) represent exocytosis events. These exocytotic profiles were only rarely observed.
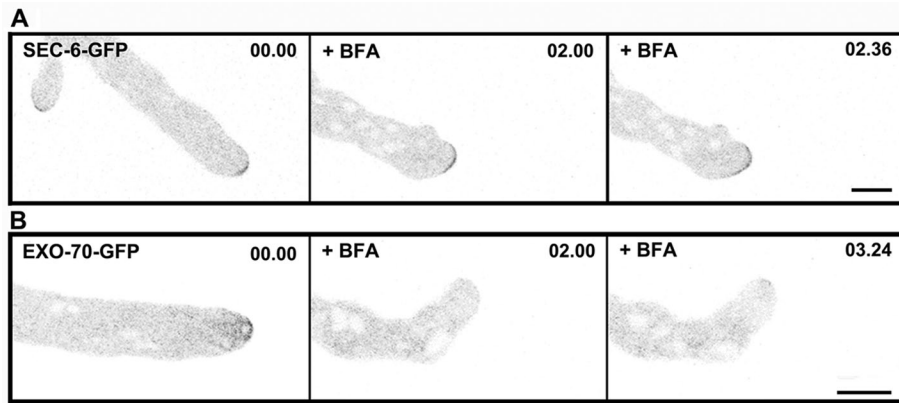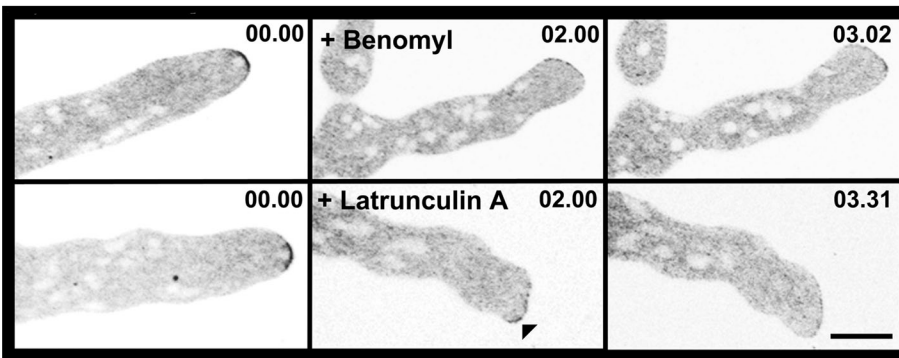
FIGURE 6: Effects of secretory pathway inhibitor brefeldin A (BFA) on localization of SEC-6-GFP and EXO-70-GFP. (A) SEC-6-GFP remains localized at the apical plasma membrane after BFA treatment. (B) EXO-70-GFP does not reach the Spitzenkörper in the presence of BFA. Scale bars, 10 μm. Time in minutes:seconds.

An organized Spitzenkörper was not recognized in hyphae of the sec-5[7-9] mutant strain (Figure 9E), although at the apex of some hyphae a differentiated spherical zone was noted (Figure 9E). This zone contained a granular-to-fibrous matrix within which only a few microvesicles were embedded (Figure 9F). The differentiated spherical zone was similar in size, location, and content to the Spitzenkörper core noted in wild-type hyphae (Figure 9A). In the mutant a massive number of macrovesicles occupied the cytoplasm (Figure 9, A and E). Macrovesicles on average were slightly larger in diameter (88 nm,

$n = 252$; SD = 9.2) and contained a more diverse content, ranging from electron dense to translucent with varying degrees of granularity. In addition, larger bodies ranging from 100 to 350 nm in diameter were also observed in the cytoplasm of the mutant. Few microvesicles could be observed in the differentiated apical spherical zone in the sec-5[7-9] mutant, and these were similar to those observed in wild type. Mitochondria, endoplasmic reticulum, and other inclusions were observed among vesicles in subapical regions of hyphae (Figure 9, E and G).

To further investigate the nature of the spherical zone found by transmission electron microscopy at apices of the sec-5[7-9] mutant, we expressed Lifeact-GFP in the mutant. By the same approach, actin was previously found at N. crassa Spitzenkörper, forming patches in the subapical collar and as cables (Berepiki et al., 2010; Delgado-Alvarez et al., 2010). In sec-5[7-9], however, Lifeact-GFP did not accumulate at the Spitzenkörper or as patches in the subapical collar (Supplemental Figure S6). Instead, it was observed as thick actin bundles that depolymerized after exposure to latrunculin A (Supplemental Figure S6). To confirm the importance of an intact exocyst for Spitzenkörper organization, we expressed SEC-6-GFP and EXO-70-GFP in sec-5[7-9] background. Both SEC-6-GFP and EXO-70-GFP were completely mislocalized in sec-5[7-9] and thus no longer observed at the apical hyphal surface or Spitzenkörper outer layer, respectively (Figure 10).

DISCUSSION

One of our long-term goals is the mechanistic understanding of how secretory vesicles are concentrated at sites of growth and how they are distributed from there to their final destination at the PM. We previously showed that the Spitzenkörper of N. crassa is a multilayered structure, with centered chitin synthase–containing microvesicles (chitosomes) and peripheral glucan synthase activity–containing macrovesicles (Verdin et al., 2009). In this study we identified association of the exocyst complex with a population of secretory vesicles, suggesting that the exocyst is involved in the PM tethering of the vesicles concentrated at the Spitzenkörper. We did not detect any exocyst component in the Spitzenkörper core region. Therefore it remains elusive how microvesicles occupying the Spitzenkörper core reach the PM. The genome sequence of N. crassa, like that of other filamentous fungi that have a high secretory capacity, revealed the existence of additional secretion-related Rab and Arf genes (e.g., ARF6/Rab2/5/18) with no homologues in yeast (Borkovich et al., 2004). Moreover, deletion of the sec4 homologue, srgA, is not lethal in Aspergillus niger (Punt et al., 2001). Taken together, the evidence suggests the

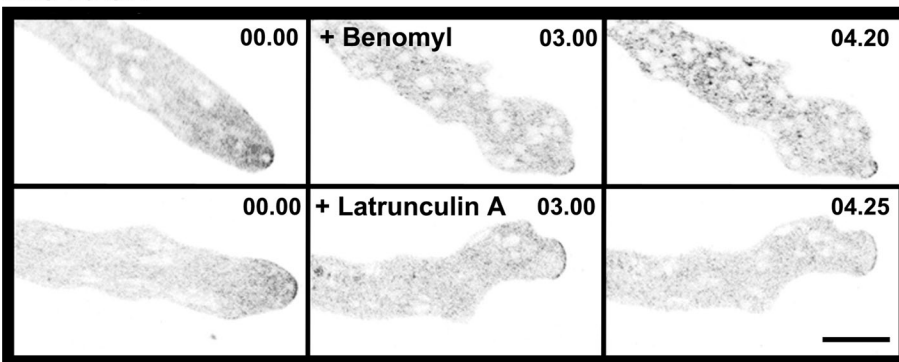## SEC-6-GFP

EXO-70-GFP

FIGURE 7: Effect of cytoskeleton inhibitors on distribution of SEC-6-GFP and EXO-70-GFP. (A) SEC-6-GFP localization at the apex is disturbed partially by the action of both benomyl and latrunculin A. (B) EXO-70-GFP is no longer found at the Spitzenkörper periphery in cells exposed to both benomyl and latrunculin A. Scale bars, 10 μm. Time in minutes:seconds.
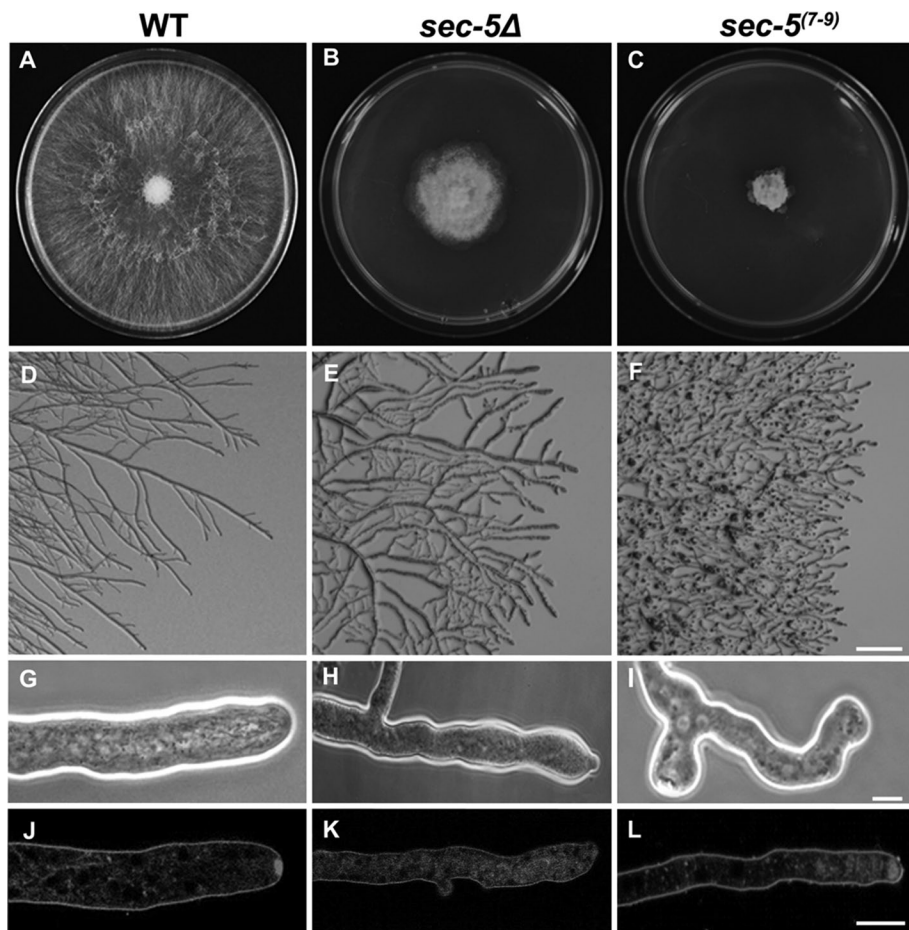
FIGURE 8: Comparison of *N. crassa* WT and *sec-5* mutant phenotypes. (A–C) After 7 d of incubation (28°C) on a Petri dish, both *sec-5Δ* and *sec-5*(7-9) mutants formed small, button-like colonies of a much smaller diameter than WT, which covered the Petri dish in 3 d (D–I). At low magnification, *sec-5* mutants showed hyperbranched and distorted hyphae. The *sec-5* mutants did not show a Spitzenkörper under phase-contrast microscopy (H, I) or when stained with FM4-64 (J–L). Scale bars, 200 µm (F), 5 µm (I),10 µm (L).

existence of additional secretory routes in filamentous fungi that are missing in yeast.

Exocyst complexes are present as two major subcomplexes of different composition in mammalian cells and budding yeast. Our localization experiments also suggest the existence of two dynamic assemblies, although it has been impossible to isolate them separately by biochemical means, not just in *N. crassa*, but also in other organisms. SEC-5, SEC-6, SEC-8, and SEC-15 accumulate as a crescent at the foremost apical region of the hyphal PM, in front of the Spitzenkörper, whereas EXO-70 and EXO-84 accumulate at the frontal region of the outer macrovesicular layer of the Spitzenkörper (Figure 11, A and B). SEC-3 adopts an intermediate position between both putative assemblies. This is quite different from the situation in yeast, in which Sec3p and Exo70p are associated with the PM, and in mammals, in which additional exocyst components are associated with the PM (Boyd *et al.*, 2004; Wang and Hsu, 2006). Our GFP-trap experiments followed by MS analyses did not reveal the existence of large quantities of stable subcomplexes in *N. crassa*, as each bait component recovered the whole octameric complex. Thus more specific approaches are necessary to characterize these subcomplexes by biochemical means. Moreover, our MS analyses also showed that presumably functionally interacting proteins, such as the predicted Rho and Rab-type GTPases (Borkovich *et al.*, 2004),

were not recovered by this approach, suggesting that they only interact in a weak or dynamic manner with specific exocyst subunits.

EXO-70 and EXO-84 associate with the Spitzenkörper in *N. crassa* hyphae regardless of their growth rate. This contrasts with observations in *A. gossypii* (Köhli *et al.*, 2008) but may be explained by the fact that the growth rates of this fungus (0.2–3.5 µm/min) are one to two magnitudes slower than that of *N. crassa* (Seiler and Plamann, 2003). This hypothesis is supported by the fact that all exocyst components form a crescent at the apical PM in *N. crassa* germlings, as in *A. gossypii*'s slow-growing hyphae. This could be due to the fact that no Spitzenkörper (apical vesicle cluster) can be seen in *N. crassa* until the germling reaches maturity and a certain growth rate (Araujo-Palomares *et al.*, 2007, 2009). Therefore we propose that the differential localization of the exocyst components in different fungal species is due to the fact that in slow-growing *N. crassa* germlings, *A. gossypii*, *S. cerevisiae*, and *C. albicans* yeast cells and pseudohyphae no Spitzenkörper exists (Köhli *et al.*, 2008).

The positional changes of the exocyst components mirrored the positional changes of the Spitzenkörper, confirming a link between the Spitzenkörper vesicles containing cell wall–synthesizing enzymes and the target PM region, where vesicles are delivered and fuse to PM as previously suggested (Bartnicki-García *et al.*, 1995; Riquelme *et al.*, 1998). Recently a role for the exocyst in determining where the cell wall–synthesizing enzymes are delivered in the PM has been proposed in *C. albicans* (Caballero-Lima *et al.*, 2013). In addition, our results indicate that the region of exocyst-mediated vesicle fusion at the hyphal apical PM follows a tip-high gradient as seen for the target-SNARE SSO-2 (Gupta and Heath, 2000) and as predicted earlier by the vesicle supply center model (Figure 11C) to be sufficient to generate the hyphal shape (Bartnicki-García *et al.*, 1989).

In *S. cerevisiae*, the exocyst components associated with secretory vesicles are transported to the cell surface in an actin-dependent manner (Finger *et al.*, 1998; Pruyne *et al.*, 1998). In *N. crassa*, transport of secretory vesicle–associated component EXO-70 and PM-associated component SEC-6 was dependent on both actin and MTs, in line with the dependence of long-distance transport on both cytoskeletal elements in filamentous fungi (Seiler *et al.*, 1997; Harris *et al.*, 2005; Steinberg, 2007). Analyses in animal cells also suggest a functional interaction between the exocyst and MTs (Vega and Hsu, 2001; Wang *et al.*, 2004). One of the possible roles suggested for the exocyst in animal cells is the regulation of vesicle release from MTs to cortical actin for vesicle docking and fusion (Wang and Hsu, 2006), which would fit with previously proposed models of vesicle traffic in fungal hyphae (Bartnicki-García, 2002; Harris *et al.*, 2005), in which the Spitzenkörper was suggested to be a switching station from MTs to actin cables. It remains to be proven whether the exocyst has a role in executing the switch.
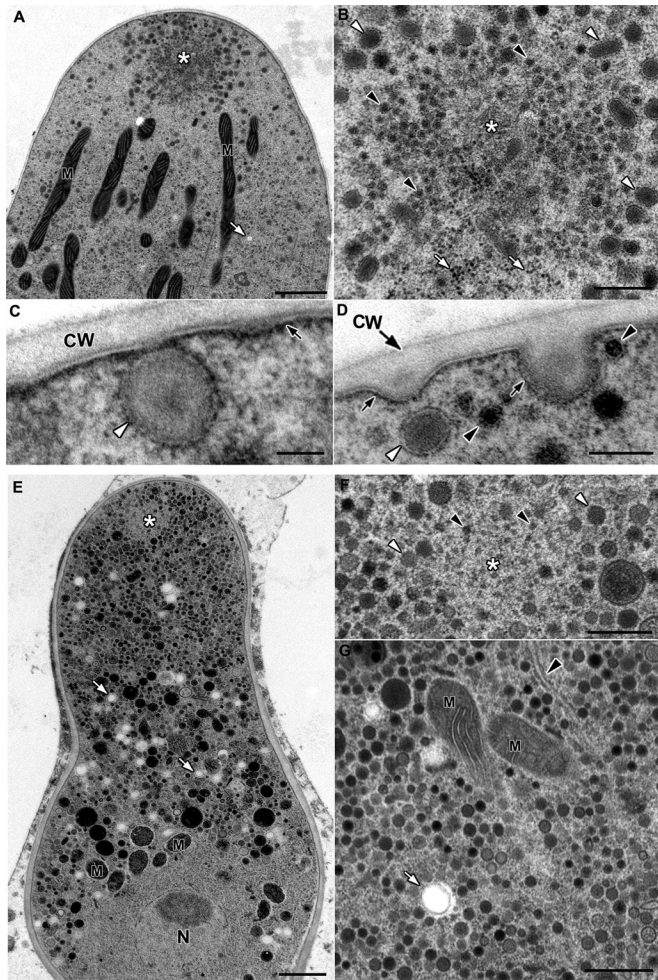
FIGURE 9: Transmission electron microscopy of cryofixed and freeze-substituted wild-type (A–D) and *sec-5*[(7-9)] mutant (E–G) hyphae of *N. crassa*. (A) Near-median longitudinal section through hyphal apex illustrating the Spitzenkörper (asterisk). Mitochondria (M) and electron-transparent vesicle (arrow) are noted. Scale bar, 1 μm. (B) Enlarged view of Spitzenkörper core (asterisk) shown in A, pointing out macrovesicles (white arrowheads), microvesicles (black arrowheads), and ribosomes (white arrows). Scale bar, 250 nm. (C) Apex of hypha with macrovesicle (arrowhead) docked at plasma membrane (arrow) just before exocytosis. Cell wall (CW) is identified. Scale bar, 40 nm. (D) Sites of exocytosis at hyphal apex shown by invaginations of PM (arrows). Macrovesicles (white arrowhead) and microvesicles (black arrowheads) are in close proximity to PM. Cell wall (CW) is pointed out. Scale bar, 100 nm. (E) Hyphal tip of *sec-5*[(7-9)] mutant showing accumulation of macrovesicles and other cytoplasmic structures. A differentiated spherical region void of most vesicles is present at apex (asterisk). Electron-transparent macrovesicles (arrows), mitochondria (M), and nucleus (N) are noted. Scale bar, 1 um. (F) Enlargement of an apex from a different cell than the one presented in E, showing a differentiated spherical region (asterisk), very few microvesicles (black arrowheads), and macrovesicles (white arrowheads). Scale bar, 300 nm. (G) Cluster of macrovesicles and additional cytoplasmic inclusions in subapical region of hypha. Note electron-transparent vesicles (arrow), mitochondria (M), and endoplasmic reticulum (arrowhead). Scale bar, 0.5 μm.

Except for Sec3p, all *S. cerevisiae* genes encoding exocyst components are essential (Novick *et al.*, 1980). Conditional loss-of-function mutants showed decreased exocytosis and accumulation of secretory vesicles in the cytoplasm (Novick *et al.*, 1980; Munson and

Novick, 2006). In *C. albicans*, deletion of Sec3 is also not lethal and leads to accumulation of vesicles in yeast buds; here, Sec3 is required for polarized growth in hyphae (Li *et al.*, 2007). We determined that most subunits are also essential for viability in *N. crassa*. This conclusion is based on the lack of homokaryotic knockout strains for most components and our inability to construct such strains (unpublished data). In contrast, *sec-5* mutants are viable but severely affected. Lack of SEC-5 impairs exocyst function and leads to accumulation of exocytic macrovesicles in the cytoplasm, decreased growth rate, induction of multiple new tips, and hyperbranching, illustrating the importance of the exocyst for Spitzenkörper formation and organization, polarized growth, and hyphal morphology.

In summary, this work shows that *N. crassa* is an excellent model system to analyze exocytosis and elucidate the role of the exocyst in polarized growth. Unlike other model systems, in which the analysis of loss-of-function mutants was required to identify the function of the exocyst, *N. crassa* allows direct manifestation of exocyst cycling between vesicles and target PM. More important, the present study suggests the existence of different mechanisms regulating the exocytosis of different cargo-transporting vesicles.

MATERIALS AND METHODS

Strains and culture conditions

Host strains for tagged exocyst components were *N. crassa* strains FGSC9718 (NMF263; Δ*mus-51::bar*[+]) and FGSC9717 (N2928, Δ*mus-51::bar*[+]*his-3*; Ninomiya *et al.*, 2004; Colot *et al.*, 2006). Culture conditions and *Neurospora* methods are described elsewhere (Davis, 2000). Strains were grown on Vogel's minimal medium (VMM; Vogel, 1956) supplemented with 1.5% sucrose. To select putative transformants, VMM supplemented with 0.05% fructose, 0.05% glucose, and 2% sorbose (FGS) and hygromycin B (Hyg, 200 μg/ml; Invitrogen, Carlsbad, CA) was used. An *N. crassa sec-5* mutant (strain 7-9) was previously obtained by UV mutagenesis (Seiler and Plamann, 2003). An *N. crassa sec-5 his-3* mutant strain was generated by crossing *sec-5*[7-9] to N625. Deletion mutants of *sec-5* (FGSC11526), *sec-8* (FGSC11510), *sec-10* (FGSC11723), *sec-15* (FGSC11509), *exo-70* (FGSC11414), and *exo-84* (FGSC11506) were generated by the *N. crassa* functional genome project (Colot *et al.*, 2006) and obtained from the Fungal Genetics Stock Center (FGSC; Kansas City, MO). Heterokaryotic mutant strains were backcrossed to Δ*sad-2* strains (SMRP277 and SMRP278) on synthetic crossing medium (Westergaard and Mitchell, 1947) to isolate homokaryotic deletion strains; *sad-2* mutants were used to circumvent the possibility of meiotic silencing (Shiu *et al.*, 2001). Progeny were screened by PCR to identify homokaryons lacking the various exocyst genes. All strains are listed in Table 3. Plasmids VMRP27-3 and VMRP28-6 containing *sec-6::8xGly::mchfp* and *exo-70::8Gly::mchfp*, respectively, cloned into *Xba*I- and *Pac*I-digested pJV15-2 (Verdín *et al.*, 2009) were transformed into *N. crassa* strain FGSC9717. Plasmid pRM49-OC30 (Delgado-Alvarez *et al.*, 2010) containing Lifeact-GFP was transformed into *N. crassa sec-5* mutant strain (SMRP33). *N. crassa his-3 sec-5* mutant strain (SMRP32) was crossed with strains expressing either SEC-6-GFP or EXO-70-GFP.

Generation of C-terminal GFP fusions

Genomic DNA from *N. crassa* WT (FGSC988) was extracted either with a DNeasy Plant Mini Kit (Qiagen, Valencia, CA) or according to a previously published method (Pomraning *et al.*, 2009). Plasmids pMF272 (Freitag *et al.*, 2004) and pGFP::hph::loxP (Honda and Selker, 2009; GenBank accession number FJ457011) were purified with plasmid isolation kits (Qiagen).

Number	Genotype	Reference or source	Number	Genotype	Reference or source
N1	*mat a*	FGSC988	SMRP6	*mat A; sec-5[7-9]*	Seiler and Plamann (2003)
N150	*mat A*	FGSC2489			
N625	*mat a; his-3*	FGSC6525	SMRP32	*mat a; his-3; sec5[7-9]*	This study
N39	*mat A; fl*	FGSC4317	NMF562	*mat A; his-3; sec-3::sgfp::hph[+]Δmus51::bar[+]*	This study
N40	*mat a; fl*	FGSC4347			
SMRP25	*mat a; Δmus-51::bar[+]*	NMF263, FGSC9718	NMF563	*mat A; his-3; sec-5::sgfp::hph[+]Δmus51::bar[+]*	This study
SMRP24	*mat A; his-3; Δmus-51::bar[+]*	N2928, FGSC9717	NMF564	*mat A; his-3; sec-6::sgfp::hph[+]Δmus51::bar[+]*	This study
NES2.11	*mat A; chs-1::sgfp[+]::hph[+]*	Sánchez-León et al. (2011)	NMF577[a]	*mat A; his-3; sec-8::sgfp::hph[+]Δmus51::bar[+]*	This study
SMRP52[a]	*mat a; chs-1::sgfp[+]::hph[+]*	Sánchez-León et al. (2011)	NMF565	*mat A; his-3; exo-70::sgfp::hph[+]Δmus51::bar[+]*	This study
NJV4.2.1	*mat A; gs-1[+]::sgfp[+]::hph[+]*	Verdín et al. (2009)	NMF566	*mat A; his-3; exo-84::sgfp::hph[+]Δmus51::bar[+]*	This study
TJV12.1[a]	*mat A; chs-1::mchfp[+]::hph[+]*	Verdín et al. (2009)	NMF578[a]	*mat A; his-3; sec-15::sgfp::hph[+]Δmus51::bar[+]*	This study
SMRP277	*mat A; Δsad-2::hph[+]*	N3400, NMF160	SMRP293[a]	*mat a; his-3[+]; sec5[7-9]; Lifeact::gfp[+]*	This study
			XEB148	*mat a; his-3[+]; sec5[7-9]; sec-6::gfp[+]*	This study
SMRP278	*mat a; Δsad-2::hph[+]*	N3401, NMF161	XEB149	*mat a; his-3[+]; sec5[7-9]; exo-70::gfp[+]*	This study
			SMRP294[a]	*mat A; his-3[+];sec-6::mchfp[+]*	This study
SMRP56	*mat a; Δsec-5*	FGSC11526	SMRP295[a]	*mat A; his-3[+];exo-70::mchfp[+]*	This study
SMRP257[a]	*mat a; Δsec-8*	FGSC11510	TEB110.1[a]	*mat A; his-3[+];exo-70::mchfp[+]; exo-70::sgfp::hph[+]Δmus51::bar[+]*	This study
SMRP258[a]	*mat a; Δsec-10*	FGSC11723			
SMRP62[a]	*mat a; Δsec-15*	FGSC11509	TEB108.1[a]	*mat A; his-3[+];exo-70::mchfp[+]; sec-6::sgfp::hph[+]Δmus51::bar[+]*	This study
SMRP137	*mat a; Δexo-70*	FGSC11414	TEB109.1[a]	*mat A; his-3[+];sec-6::mchfp[+]; exo-70::msgfp::hph[+]Δmus51::bar[+]*	This study
SMRP138[a]	*mat a; Δexo-84*	FGSC11506			

Some strains were obtained from the Fungal Genetics Stock Center (FGSC), Kansas City, MO.
[a]Heterokaryon.

TABLE 3: *N. crassa* strains used.

We searched the *N. crassa* genome sequence for orthologues of all known exocyst components previously identified in yeast (Table 1) and designed primers to tag the endogenous genes with super-folder GFP by a split marker gene replacement procedure (Smith et al., 2011). Six primers were designed for each replacement cassette (Table 4). We followed a standard naming convention for each gene to be tagged, where forward and reverse primers "gene"GlyF and "gene"GlyR, respectively, amplify ~1 kb upstream of each open reading frame. Primers designated "gene"GlyR are reverse primers to the ~20 nucleotides (nt) at the 3' end of each coding region immediately upstream of the stop codon and preceded by 30 nt of the 5'-most sequence of the tags, usually a linker sequence of 10 glycine residues (Honda and Selker, 2009). Primers "gene"LoxF and "gene"LoxR amplify ~1 kb downstream of the coding region of interest, sometimes interrupting the 3' untranslated region. Primers designated "gene"LoxF are forward primers to ~30 nt of the
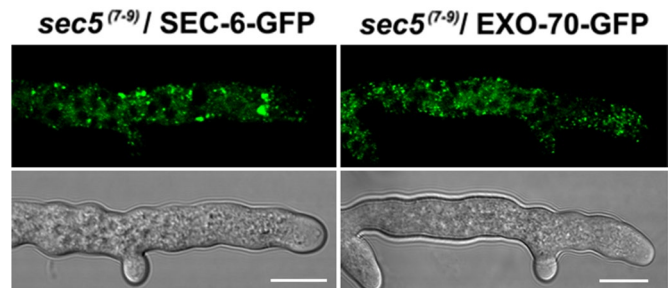

FIGURE 10: Localization of SEC-6-GFP and EXO-70-GFP in *N. crassa* sec-5[(7-9)] mutant. Fluorescence was observed at neither the apical plasma membrane (SEC-6-GFP; top left) nor the Spitzenkörper outer layer (EXO-70-GFP; top right). Instead, fluorescence was observed as foci throughout the cytoplasm. Bottom row, corresponding differential interference contrast images. Scale bar, 10 μm.
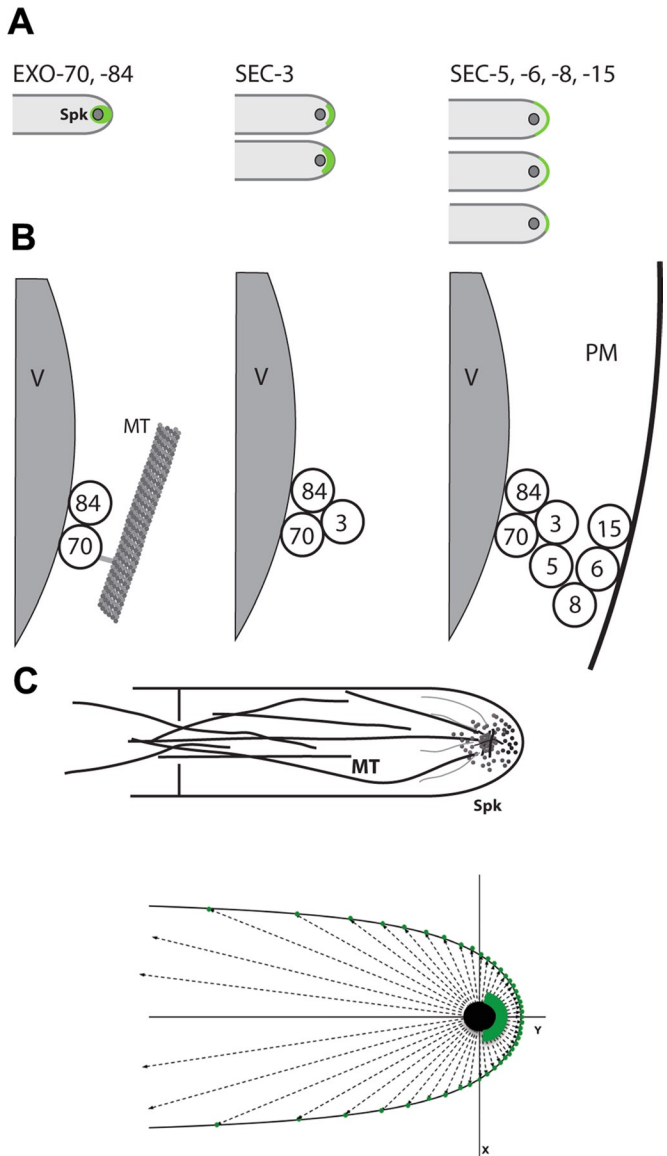
FIGURE 11: Model for distribution of exocyst components at the hyphal apex and septa and their role in vesicle delivery. (A) GFP fluorescence distribution of different labeled exocyst subunits, grouped by pattern. Exocyst components SEC-5, -6, -8, and -15 localize at the PM of the apical dome, occupying a somewhat variable region. SEC-3 is found at the region between the Spitzenkörper and the apical PM. EXO-70 and -84 associate with secretory vesicles concentrated in the Spitzenkörper outer layer proximal region, presumably leaving the Spitzenkörper and going on to fuse with the PM. (B) Model for distribution of the different exocyst components during tethering of a vesicle with the plasma membrane. (C) Top, the Spitzenkörper localizes around a bundle of microtubules. Bottom, modification of the vesicle supply center (VSC) model for fungal morphogenesis (Bartnicki-García *et al.*, 1989), where SEC-5, -6, -8, and -15 localize at the PM at the area of predicted maximum exocytosis, which corresponds to the region of maximum fluorescence in the analyzed strains. The VSC corresponds to the Spitzenkörper in real cells, composed of a core of chitin synthase–containing microvesicles and an outer layer of macrovesicles, some containing glucan synthase activity as described earlier (Verdín *et al.*, 2009).

3′-most sequence in the tag cassettes, typically including a LoxP site for the Cre recombinase (Honda and Selker, 2009), followed by 20 nt of sequence directly downstream of the coding region of

interest. Primers 10xGlyF and LoxPR amplify cassettes that carry various tags or antibiotic-resistance markers.

To generate replacement cassettes, primers "gene"GlyF and "gene"GlyR, or "gene"LoxF and "gene"LoxR, respectively, were used to amplify the 5′ and 3′ flanks for gene replacements with wild-type *Neurospora* genomic DNA as template. Amplicon 1 (5′PCRp1) and amplicon 2 (3′PCRp2) were gel purified and used as templates for a second round of PCR, where 5′PCRp1 and 3′PCRp2 were individually mixed with different tag and marker cassette amplicons (TagPCRp3). Primers used for this second PCR were "gene"GlyF and hphSMR, or hphSMF and "gene"LoxR (Supplemental Figure S1). The resulting fragments were gel purified, mixed in equal proportions (~0.5 µg DNA/transformation), and used to transform *Neurospora* conidia by electroporation (~2.5×10^9 cells/ml, 1.5 kV, 600 Ω, 25 µF; Margolin *et al.*, 1997). Successful transformation is believed to require three homologous recombination events (between the 5′ flank and the 3′ flank of the genomic sequence and the two PCR fragments, as well as the overlapping region of the marker sequence—this last event reconstitutes the selectable marker).

Host strains for transformations were NMF263 (FGSC9718) and N2928 (FGSC9717). Electroporated conidia were plated on VMM with FGS, histidine (His), and Hyg (200 or 300 µg/ml). Primary transformants were picked into slants with His and Hyg or grown on VMM plates with His and Hyg (100 µg/ml). Transformants with fluorescence detected under an epifluorescence or confocal microscope were chosen for further analysis.

Mass spectrometry and database analysis

Liquid *N. crassa* cultures were grown at room temperature, harvested gently by filtration using a Büchner funnel, and ground in liquid nitrogen. The pulverized mycelium was mixed 1:1 with standard IP buffer (50 mM Tris/HCL pH 7.5, 100 mM KCl, 10 mM MgCl$_2$, 0.15% NP-40, 5 mM NaF, 1 mM PEFA, 1 mM Na$_3$VO$_4$, 25 mM β-glycerophosphate, 2 mM benzamidine, 2 ng/µl pepstatin A, 10 ng/µl aprotinin, 10 ng/µl leupeptin) and centrifuged (1 h, 10,000 rpm, Sorvall SS34 rotor) to obtain crude cell extracts as previously described (Dettmann *et al.*, 2012; Maerz *et al.*, 2012). The cell extracts were incubated with 2 µl GFP trap beads (ChromoTek GmbH, Planegg-Martinsried, Germany)/15 ml of cell extract on a rotator for 2 h at 4°C. The beads were washed three times with IP buffer, and immunoprecipitated proteins were recovered by boiling the beads for 10 min at 98°C in Laemmli buffer and separated by SDS–PAGE.

For protein identification by mass spectrometry, peptides of the in-gel trypsinated proteins were extracted from gel slices of Coomassie-stained protein bands. Peptides of a 5 µl-sample solution were trapped and washed with 0.05% trifluoroacetic acid on an Acclaim PepMap 100 column (75 µm × 2 cm, C18, 3 µm, 100 Å, P/N164535; Thermo Scientific, Waltham, MA) at a flow rate of 4 µl/min for 12 min. Analytical peptide separation by reverse-phase chromatography was performed on an Acclaim PepMap RSLC column (75 µm × 15 cm, C18, 3 µm, 100 Å, P/N164534; Thermo Scientific) running a gradient from 96% solvent A (0.1% formic acid) and 4% solvent B (acetonitrile, 0.1% formic acid) to 50% solvent B within 25 min at a flow rate of 250 nl/min (solvents and chemicals were from Fisher Chemicals, Fair Lawn, NJ; HPLC grade). Peptides eluting from the chromatographic column were on-line ionized by nanoelectrospray using the Nanospray Flex Ion Source (Thermo Scientific) and transferred into the mass spectrometer. Full scans within $m/z = 300$–1850 were recorded by the Orbitrap-FT analyzer at a resolution of 60,000 at $m/z = 400$. Each sample was analyzed using two different fragmentation techniques applying a data-dependent

Name	Sequence
hphSMR	5'-TCGCCTCGCTCCAGTCAATGACC-3'
hphSMF	5'-AAAAAGCCTGAACTCACCGCGACG-3'
10xGlyF	5'-GGCGGAGGCGGCGGAGGCGGAGGCGGAGG-3'
loxPR	5'-CGAGCTCGGATCCATAACTTCGTATAGCA -3'
sec5GlyR	5'-CCTCCGCCTCCGCCTCCGCCGCCTCCGCCCCTCTCGCTCCCCGTAGTCCC-3'
sec5loxF	5'-TGCTATACGAAGTTATGGATCCGAGCTCGGTGGGAAGAAGTAACTCTGTCTTG-3'
sec5GlyF	5'-CGTGCCAGCCCACCACGTTCACCA-3'
sec5loxR	5'-GTGCCATGGGCGGCGCAGGAAGCG-3'
sec10loxR	5'-CAGTCGCAAACCCAGACCCAGACC-3'
sec10loxF	5'-TGCTATACGAAGTTATGGATCCGAGCTCGAAGATATTGCGAGTTTTGGTGGGG-3'
sec10GlyF	5'-CGATTCGTCAGACCTTACGCCCAC-3'
sec10GlyR	5'-CCTCCGCCTCCGCCTCCGCCGCCTCCGCCCAGTCCAGCCAGTACACCCTGGATACC-3'
sec8loxR	5'-GTGTTGACTTTTGTCCAATGATCG-3'
sec8loxF	5'-TGCTATACGAAGTTATGGATCCGAGCTCGGATTTGCAGGACATTTAGACTTGG-3'
sec8GlyF	5'-GAGGTGAACCAGCTCATCGCGTGG-3'
sec8GlyR	5'-CCTCCGCCTCCGCCTCCGCCGCCTCCGCCAGACTGCCACATGTACTCGCTCAA-3'
sec6loxR	5'-ACTGATGATCAAGCTCAAGAAACC-3'
sec6loxF	5'-TGCTATACGAAGTTATGGATCCGAGCTCGGGGGGACACGCAATAGTTATCCTGG-3'
sec6GlyF	5'-ATGACCAAGTTGGGAATGAAGCAG-3'
sec6GlyR	5'-CCTCCGCCTCCGCCTCCGCCGCCTCCGCCTTTGACCTTGCTCATGATAGTTTC-3'
sec3loxR	5'-AAATGGCCAGATTTGTCAAATGCGGTG-3'
sec3loxF	5'-TGCTATACGAAGTTATGGATCCGAGCTCGTTGAGATGGTCAGAAGGAGAGAGG-3'
sec3GlyF	5'-AGAAGCGCAAAGGCGTCATCCACT-3'
sec3GlyR	5'-CCTCCGCCTCCGCCTCCGCCGCCTCCGCCCCTCCCCACTTGGGTAAAAGCACT-3'
exo84loxR	5'-CTTTGTCACTGAATCAAAGACGGC-3'
exo84GlyF	5'-AACCGGAGACTCGTCAAATGGCCG-3'
exo70loxR	5'-ATCATGATTGTAGAGAGTCATGAG-3'
exo70GlyF	5'-AACTGAACAGCCACATCAAGTCGC-3'
exo84loxF	5'-TGCTATACGAAGTTATGGATCCGAGCTCGGCTGCAAAGACAGAGGATCTA-3'
exo84GlyR	5'-CCTCCGCCTCCGCCTCCGCCGCCTCCGCCGGACAGACCCAGCCCAGCCGA-3'
exo70loxF	5'-TGCTATACGAAGTTATGGATCCGAGCTCGGCGGTACATTCGGATCAGGGC-3'
exo70GlyR	5'-CCTCCGCCTCCGCCTCCGCCGCCTCCGCCGTAAAGACTGCGGAAAACAGC-3'
sec6-XbaI-C-mChFP-F	5'-GCTCTAGAATGGACTTACCGCCCGTCAAC-3'
sec6-PacI-8xgly-C-mChFP-R	5'-CCTTAATTAAGCCGCCTCCGCCGCCTCCGCCGCCTTTGACCTTGCTCATGATAG-3'
exo70-XbaI-C-mChFP-F	5'-GCTCTAGAATGGCTGTCGGCCTCATCAAC-3'
exo70-PacI-8xgly-C-mChFP-R	5'-CCTTAATTAAGCCGCCTCCGCCGCCTCCGCCGCCGTAAAGACTGCGGAAAACAGCAGCG-3'

TABLE 4: Oligonucleotides used.

top five experiment: collision-induced decay with multistage activation and readout in the LTQ Velos Pro linear ion trap, and higher-energy collision dissociation and subsequent readout in the Orbitrap-FT analyzer. LC/MS method programming and data acquisition was performed with XCalibur 2.2 (Thermo Scientific). Orbitrap raw files were analyzed with Proteome Discoverer 1.3 (Thermo Scientific) using the Mascot and Sequest search engines against the *N. crassa* protein database with the following criteria: peptide mass tolerance, 10 ppm; MS/MS ion mass tolerance, 0.8 Da; and up to two missed cleavages allowed.

Light microscopy

Observations of growing cells (germlings or mature hyphae) were performed as previously described (Sánchez-León *et al.*, 2011; Richthammer *et al.*, 2012) using a Zeiss LSM-510 META inverted laser scanning confocal microscope (Carl Zeiss, Jena, Germany) and an Olympus FluoView FV1000 Confocal Microscope (Olympus, Japan), both equipped with Ar/2 ion and He/Ne1 lasers to detect GFP (λ_{ex} = 488, λ_{em} = 505–530 nm) and mChFP (λ_{ex} = 543, λ_{em} = 600–630 nm). We used a Plan Neofluar 100× oil immersion objective (numerical aperture 1.3) and a Plan Apochromat 60× oil

immersion objective (numerical aperture 1.42). The images were obtained in all channels simultaneously and handled digitally with LSM-510, version 3.2, software (Carl Zeiss) and with Olympus Fluo view software (Version 4.0a).

For total internal reflection fluorescence microscopy (TIRFM), an IX-70 inverted microscope equipped with a 60×/1.45 Apochromat objective lens (Olympus America, Center Valley, PA) and a krypton/argon laser (488 nm; Melles Griot, Carlsbad, CA) was used. Images were recorded with a Cascade 512B electron-multiplying, charge-coupled device camera (Photometrics, Tucson, AZ) for 2–3 min at 512×512 resolution and 10 frames/s. MetaMorph 6.1 software (Universal Imaging, Downingtown, PA) was used to control the camera and capture images. MetaMorph 7.5.0 was used to analyze and process TIRFM time series.

Because germ tubes have a tendency to grow into the agar, making microscopy difficult for the analyses of germlings, we inoculated conidia of each strain into VMM plates containing 3% agar to force conidia to germinate on top of the medium surface and observed them by laser scanning confocal microscopy after 6, 7, 8, and 9 h of incubation.

Transmission electron microscopy

Actively growing hyphae were prepared for transmission electron microscopy using cryopreparation methods. Cells were grown on thin, sterile, deionized dialysis membrane segments overlaying VCM at 23°C. After ~24 h of growth, cells and supporting membranes were trimmed with a sharp razor blade to ~5 × 5 mm and after 30–40 min (time to recover from trimming) were removed from the agar surface and immediately cryofixed by rapid plunging into liquid propane cooled to –186°C with liquid nitrogen (Roberson and Fuller, 1988; McDaniel and Roberson, 2000). Freeze substitution took place in 1% glutaraldehyde and 1% tannic acid (wt/vol) in anhydrous acetone at –85°C for 72 h. After washing in cold acetone (–85°C), the samples were warmed slowly to room temperature in 1% OsO_4 (wt/vol) in acetone, washed in acetone, and infiltrated and flat embedded in Spurr's resin (Spurr, 1969). Selected hyphae were sectioned and poststained in 2% uranyl acetate in 50% ethanol and Sato's lead citrate (Hanaichi *et al.*, 1986). Sections were examined using an FEI CM12S transmission electron microscope (FEI Electronics Instruments, Mahwah, NJ) at 80 kV coupled to a Gatan 689 CCD digital camera (1024 × 1024 pixel area; Gatan, Pleasanton, CA). Final figures were assembled using Photoshop 7.0 (Adobe, San Jose, CA).

Growth and fluorescence measurements

Growth rate of each hypha was calculated from recorded time series by using both the LSM-510 software and ImageJ (National Institutes of Health, Bethesda, MD) and measuring the distance traveled by the hypha over time. The arc of fluorescence occupied by the corresponding tagged exocyst component at the hyphal apex was measured on ImageJ using the Angle tool and locating the vertex of the angle behind the Spitzenkörper, from where the two rays begin until reaching either the apical plasma membrane (at the interface between fluorescence and no fluorescence) for SEC-6-GFP or the Spitzenkörper-proximal external region for EXO-70-GFP.

Intensity of fluorescence was obtained using the Profile option in the LSM-510 Image Examiner software (version 3.2) by drawing a line originating outside of the middle point of the foremost hyphal tip and ending a few micrometers behind the Spitzenkörper. Animated three-dimensional plots of fluorescence intensities of the pixels reaching the plasma membrane over time of the time series obtained by TIRFM were generated with the Surface plot plug-in of ImageJ.

Fluorescent dyes and inhibitors

For staining endomembranes, we used the styril dye *N*-(3-triethylammoniumpropyl)-4-(6-(4-(diethylamino) phenyl) hexatrienyl) pyridinium dibromide (FM4-64; 5 μM, λ = 514/670 nm absorption/emission; Molecular Probes, Invitrogen, Carlsbad, CA). A stock solution (500 μg/ml) of the anti-microtubule agent methyl 1-(butylcarbamoyl)-2-benzimidazolecarbamate (benomyl; Sigma-Aldrich, St. Louis, MO) was prepared in ethanol. A stock solution (1 mg/ml) of the actin inhibitor latrunculin A (Sigma-Aldrich) was prepared in dimethyl sulfoxide. Different concentrations of benomyl (10, 20, and 30 μg/ml) and latrunculin A (20 and 40 μg/ml) were initially tested to assess the optimal concentration at which morphological defects were visible in cells growing at a reduced growth rate. A concentration of 20 μg/ml in VMM was used thereafter for both inhibitors. To inhibit the endoplasmic reticulum–Golgi secretory pathway, brefeldin A (Sigma-Aldrich) was added to growing hyphae at a final working concentration of 20 μM in VMM from a stock solution in dimethyl sulfoxide. Agar blocks were cut from the edge of growing colonies and inverted onto coverslips containing 10 μl of the corresponding inhibitor or fluorochrome. After 10 min, they were observed by laser scanning confocal microscopy.

REFERENCES

Araujo-Palomares CL, Castro-Longoria E, Riquelme M (2007). Ontogeny of the Spitzenkörper in germlings of *Neurospora crassa*. Fungal Genet Biol 44, 492–503.

Araujo-Palomares CL, Riquelme M, Castro-Longoria E (2009). The polarisome component SPA-2 localizes at the apex of *Neurospora crassa* and partially colocalizes with the Spitzenkörper. Fungal Genet Biol 46, 551–563.

Bartnicki-García S (2002). Hyphal tip growth: outstanding questions. In: Molecular Biology of Fungal Development, ed. HD Osiewacz, New York: Marcel Dekker, 29–58.

Bartnicki-García S, Bartnicki DD, Gierz G, López-Franco R, Bracker CE (1995). Evidence that Spitzenkörper behavior determines the shape of a fungal hypha: a test of the hyphoid model. Exp Mycol 19, 153–159.

Bartnicki-García S, Hergert F, Gierz G (1989). Computer simulation of fungal morphogenesis and the mathematical basis for hyphal (tip) growth. Protoplasma 153, 46–57.

Berepiki A, Lichius A, Shoji JY, Tilsner J, Read ND (2010). F-actin dynamics in *Neurospora crassa*. Eukaryot Cell 9, 547–557.

Borkovich KA et al. (2004). Lessons from the genome sequence of *Neurospora crassa*: tracing the path from genomic blueprint to multicellular organism. Microbiol Mol Biol Rev 68, 1–108.

Boyd C, Hughes T, Pypaert M, Novick P (2004). Vesicles carry most exocyst subunits to exocytic sites marked by the remaining two subunits, Sec3p and Exo70p. J Cell Biol 167, 889–901.

Caballero-Lima D, Kaneva I, Watton S, Sudbery PE, Craven CJ (2013). The spatial distribution of the exocyst and actin cortical patches is sufficient to organize hyphal tip growth. Eukaryot Cell 12, 998–1008.

Cole RA, Synek L, Zarsky V, Fowler JE (2005). SEC8, a subunit of the putative Arabidopsis exocyst complex, facilitates pollen germination and competitive pollen tube growth. Plant Physiol 138, 2005–2018.

Colot HV, Park G, Turner GE, Ringelberg C, Crew CM, Litvinkova L, Weiss RL, Borkovich KA, Dunlap JC (2006). A high-throughput gene knockout procedure for Neurospora reveals functions for multiple transcription factors. Proc Natl Acad Sci USA 103, 10352–10357.

Davis RH (2000). Neurospora : Contributions of a Model Organism, New York: Oxford University Press.

Delgado-Alvarez DL, Callejas-Negrete OA, Gomez N, Freitag M, Roberson RW, Smith LG, Mouriño-Pérez RR (2010). Visualization of F-actin localization and dynamics with live cell markers in Neurospora crassa. Fungal Genet Biol 47, 573–586.

Dettmann A, Heilig Y, Ludwig S, Schmitt K, Illgen J, Fleissner A, Valerius O, Seiler S (2013). HAM-2 and HAM-3 are central for the assembly of the Neurospora crassa STRIPAK complex at the nuclear envelope and regulate nuclear accumulation of the MAP kinase MAK-1 in a MAK-2-dependent manner. Mol Microbiol 90, 796–812.

Dettmann A, Illgen J, Marz S, Schurg T, Fleissner A, Seiler S (2012). The NDR kinase scaffold HYM1/MO25 is essential for MAK2 MAP kinase signaling in Neurospora crassa. PLoS Genet 8, e1002950.

Elias M, Drdova E, Ziak D, Bavlnka B, Hala M, Cvrckova F, Soukupova H, Zarsky V (2003). The exocyst complex in plants. J Cell Biol 27, 199–201.

Fendrych M et al. (2010). The Arabidopsis exocyst complex is involved in cytokinesis and cell plate maturation. Plant Cell 22, 3053–3065.

Finger FP, Hughes TE, Novick P (1998). Sec3p is a spatial landmark for polarized secretion in budding yeast. Cell 92, 559–571.

Freitag M, Hickey PC, Raju NB, Selker EU, Read ND (2004). GFP as a tool to analyze the organization, dynamics and function of nuclei and microtubules in Neurospora crassa. Fungal Genet Biol 41, 897–910.

Galagan JE et al. (2003). The genome sequence of the filamentous fungus Neurospora crassa. Nature 422, 859–68.

Grindstaff KK, Yeaman C, Anandasabapathy N, Hsu SC, Rodriguez-Boulan E, Scheller RH, Nelson WJ (1998). Sec6/8 complex is recruited to cell-cell contacts and specifies transport vesicle delivery to the basal-lateral membrane in epithelial cells. Cell 93, 731–740.

Guo W, Grant A, Novick P (1999a). Exo84p Is an Exocyst protein essential for secretion. J Biol Chem 274, 23558–23564.

Guo W, Roth D, Walch-Solimena C, Novick P (1999b). The exocyst is an effector for Sec4p, targeting secretory vesicles to sites of exocytosis. EMBO J 18, 1071–1080.

Gupta GD, Heath IB (2000). A tip-high gradient of a putative plasma membrane SNARE approximates the exocytotic gradient in hyphal apices of the fungus Neurospora crassa. Fungal Genet Biol 29, 187–199.

Hala M et al. (2008). An exocyst complex functions in plant cell growth in Arabidopsis and tobacco. Plant Cell 20, 1330–1345.

Hanaichi T, Sato T, Iwamoto T, Malavasi-Yamashiro J, Hoshino M, Mizuno N (1986). A stable lead by modification of Sato's method. J Electron Microsc 35, 304–306.

Harris SD, Read ND, Roberson RW, Shaw BD, Seiler S, Plamann M, Momany M (2005). Polarisome meets Spitzenkörper: microscopy, genetics, and genomics converge. Eukaryot Cell 4, 225–229.

Hayakawa Y, Ishikawa E, Shoji JY, Nakano H, Kitamoto K (2011). Septum-directed secretion in the filamentous fungus Aspergillus oryzae. Mol Microbiol 81, 40–55.

Heilig Y, Schmitt K, Seiler S (2013). Phospho-regulation of the Neurospora crassa septation initiation network. PLoS One 8, e79464.

Hertzog M, Chavrier P (2011). Cell polarity during motile processes: keeping on track with the exocyst complex. Biochem J 433, 403–409.

Honda S, Selker EU (2009). Tools for fungal proteomics: multifunctional Neurospora vectors for gene replacement, protein expression and protein purification. Genetics 182, 11–23.

Hsu SC, TerBush D, Abraham M, Guo W (2004). The exocyst complex in polarized exocytosis. Int Rev Cytol 233, 243–265.

Jones LA, Sudbery PE (2010). Spitzenkörper, exocyst, and polarisome components in Candida albicans hyphae show different patterns of localization and have distinct dynamic properties. Eukaryot Cell 9, 1455–1465.

Köhli M, Galati V, Boudier K, Roberson RW, Philippsen P (2008). Growth-speed-correlated localization of exocyst and polarisome components in growth zones of Ashbya gossypii hyphal tips. J Cell Sci 121, 3878–3889.

Li CR, Lee RT, Wang YM, Zheng XD, Wang Y (2007). Candida albicans hyphal morphogenesis occurs in Sec3p-independent and Sec3p-dependent phases separated by septin ring formation. J Cell Sci 120, 1898–1907.

Maerz S, Dettmann A, Seiler S (2012). Hydrophobic motif phosphorylation coordinates activity and polar localization of the Neurospora crassa nuclear Dbf2-related kinase COT1. Mol Cell Biol 32, 2083–2098.

Margolin BS, Freitag M, Selker EU (1997). Improved plasmids for gene targeting at the his-3 locus of Neurospora crassa by electroporation. Fungal Genet Newsl 44, 34–36.

McDaniel DP, Roberson RW (2000). Microtubules are required for motility and positioning of vesicles and mitochondria in hyphal tip cells of Allomyces macrogynus. Fungal Genet Biol 31, 233–244.

Moskalenko S, Tong C, Rosse C, Mirey G, Formstecher E, Daviet L, Camonis J, White MA (2003). Ral GTPases regulate exocyst assembly through dual subunit interactions. J Biol Chem 278, 51743–51748.

Munson M, Novick P (2006). The exocyst defrocked, a framework of rods revealed. Nat Struct Mol Biol 13, 577–581.

Ninomiya Y, Suzuki K, Ishii C, Inoue H (2004). Highly efficient gene replacements in Neurospora strains deficient for nonhomologous end-joining. Proc Natl Acad Sci USA 101, 12248–12253.

Novick P, Ferro S, Schekman R (1981). Order of events in the yeast secretory pathway. Cell 25, 461–469.

Novick P, Field C, Shekman R (1980). Identification of 23 complementation groups required for post-translational events in the yeast secretory pathway. Cell 21, 205–215.

Pomraning KR, Smith KM, Freitag M (2009). Genome-wide high throughput analysis of DNA methylation in eukaryotes. Methods 47, 142–150.

Pruyne DW, Schott DH, Bretscher A (1998). Tropomyosin-containing actin cables direct the myo2p-dependent polarized delivery of secretory vesicles in budding yeast. J Cell Biol 143, 1931–1945.

Punt PJ, Seiboth B, Weenink XO, van Zeiji C, Lenders M, Konetschny C, Ram AFJ, Montijn R, Kubicek CP, van den Hondel CA (2001). Identification and characterization of a family of secretion-related small GTPase-encoding genes from the filamentous fungus Aspergillus niger: a putative SEC4 homologue is not essential for growth. Mol Microbiol 41, 513–525.

Richthammer C, Enseleit M, Sánchez-León E, Marz S, Heilig Y, Riquelme M, Seiler S (2012). RHO1 and RHO2 share partially overlapping functions in the regulation of cell wall integrity and hyphal polarity in Neurospora crassa. Mol Microbiol 85, 716–733.

Riquelme M, Gierz G, Bartnicki-García S (2000). Dynein and dynactin deficiencies affect the formation and function of the Spitzenkörper and distort hyphal morphogenesis of Neurospora crassa. Microbiology 146, 1743–1752.

Riquelme M, Reynaga-Peña CG, Gierz G, Bartnicki-García S (1998). What determines growth direction in fungal hyphae? Fungal Genet Biol 24, 101–109.

Riquelme M, Roberson RW, McDaniel DP, Bartnicki-García S (2002). The effects of ropy-1 mutation on cytoplasmic organization and intracellular motility in mature hyphae of Neurospora crassa. Fungal Genet Biol 37, 171–179.

Riquelme M et al. (2011). Architecture and development of the Neurospora crassa hypha—a model cell for polarized growth. Fungal Biol 115, 446–474.

Rizzoli SO, Jahn R (2007). Kiss-and-run, collapse and "readily retrievable" vesicles. Traffic 8, 1137–1144.

Roberson RW, Fuller MS (1988). Ultrastructural aspects of the hyphal tip of Sclerotium rolfsii preserved by freeze substitution. Protoplasma 146, 143–149.

Sánchez-León E, Verdín J, Freitag M, Roberson RW, Bartnicki-García S, Riquelme M (2011). Traffic of chitin synthase 1 (CHS-1) to the Spitzenkörper and developing septa in hyphae of Neurospora crassa: actin dependence and evidence of distinct microvesicle populations. Eukaryot Cell 10, 683–695.

Seiler S, Nargang FE, Steinberg G, Schliwa M (1997). Kinesin is essential for cell morphogenesis and polarized secretion in Neurospora crassa. EMBO J 16, 3025–3034.

Seiler S, Plamann M (2003). The genetic basis of cellular morphogenesis in the filamentous fungus Neurospora crassa. Mol Biol Cell 14, 4352–4364.

Shandala T, Kakavanos-Plew R, Ng YS, Bader C, Sorvina A, Parkinson-Lawrence EJ, Brooks RD, Borlace GN, Prodoehl MJ, Brooks DA (2012).

Molecular machinery regulating exocytosis. In: Crosstalk and Integration of Membrane Trafficking Pathways, ed. R Weigert. Available at: http://www.intechopen.com/books/crosstalk-and-integration-of-membrane-trafficking-pathways/molecular-machinery-regulating-exocytosis (accessed 3 June 2013).

Shen D, Yuan H, Hutagalung A, Verma A, Kummel D, Wu X, Reinisch K, McNew JA, Novick P (2013). The synaptobrevin homologue Snc2p recruits the exocyst to secretory vesicles by binding to Sec6p. J Cell Biol 202, 509–526.

Shiu PK, Raju NB, Zickler D, Metzenberg RL (2001). Meiotic silencing by unpaired DNA. Cell 107, 905–916.

Smith KM, Phatale PA, Sullivan CM, Pomraning KR, Freitag M (2011). Heterochromatin is required for normal distribution of Neurospora crassa CenH3. Mol Cell Biol 31, 2528–2542.

Spurr AR (1969). A low-viscosity epoxy resin embedding medium for electron microscopy. J Ultrastruct Res 26, 31–43.

Steinberg G (2007). Hyphal growth: a tale of motors, lipids, and the Spitzenkörper. Eukaryot Cell 6, 351–360.

Sudbery P (2011). Fluorescent proteins illuminate the structure and function of the hyphal tip apparatus. Fungal Genet Biol 48, 849–857.

Taheri-Talesh N, Horio T, Araujo-Bazan L, Dou X, Espeso EA, Peñalva MA, Osmani SA, Oakley BR (2008). The tip growth apparatus of Aspergillus nidulans. Mol Biol Cell 19, 1439–1449.

TerBush DR, Maurice T, Roth D, Novick P (1996). The exocyst is a multiprotein complex required for exocytosis in Saccharomyces cerevisiae. EMBO J 15, 6483–6494.

TerBush DR, Novick P (1995). Sec6, Sec8, and Secl5 are components of a multisubunit complex which localizes to small bud tips in Saccharomyces cerevisiae. J Cell Biol 130, 299–312.

Vega IE, Hsu SC (2001). The exocyst complex associates with microtubules to mediate vesicle targeting and neurite outgrowth. J Neurosci 21, 3839–3848.

Verdin J, Bartnicki-Garcia S, Riquelme M (2009). Functional stratification of the Spitzenkörper of Neurospora crassa. Mol Microbiol 74, 1044–1053.

Vogel HJ (1956). A convenient growth medium for Neurospora (Medium N). Microbial Genet Bull 13, 42–43.

Wang S, Hsu SC (2006). The molecular mechanisms of the mammalian exocyst complex in exocytosis. Biochem Soc Trans 34, 687–690.

Wang S, Liu Y, Adamson CL, Valdez G, Guo W, Hsu SC (2004). The mammalian exocyst, a complex required for exocytosis, inhibits tubulin polymerization. J Biol Chem 279, 35958–35966.

Westergaard M, Mitchell HK (1947). Neurospora. V. A synthetic medium favoring sexual reproduction. Am J Bot 34, 573–577.

Zhang Y, Liu CM, Emons AM, Ketelaar T (2010). The plant exocyst. J Integr Plant Biol 52, 138–146.